

Unsteady numerical simulation of suction side leading edge cavitation in a Francis turbine runner

Jian Chen, Xavier Escaler*

Department of Fluid Mechanics, Universitat Politècnica de Catalunya, Barcelona, Spain

*xavier.escaler@upc.edu

ABSTRACT

Cavitation appearance within the runner of the water turbines is a common problem that induces vibrations and provokes the erosion of the blades. Although many investigations have been carried out in simple configurations such as 2D and 3D hydrofoils in cavitation tunnels, few works have been done to simulate the cavitation dynamic behavior in actual turbine geometries. In this paper, the unsteady numerical simulation of suction side leading edge cavitation has been carried out for the GAMM Francis runner. For that, the two-phase model available in ANSYS® CFX and the Shear Stress Transport (SST) turbulence model have been used. A sensitivity analysis of various model parameters has been done and the results have been validated with experimental values obtained in a reduced scale model test facility at the best efficiency point. Special attention has been given to determine if a shedding process also exists and to understand the main hydrodynamic mechanisms involved. In conclusion, the instability of the leading edge cavitation seems to be mainly caused by field pressure perturbations originating from the guide vanes or the draft tube.

KEY WORDS: Francis turbine, inlet blade cavitation, unsteady flow simulation, Zwart cavitation model.

INTRODUCTION

Cavitation is a common event that occurs in hydraulic machinery, which can lead to loss of performance, lower efficiency, vibrations and noise. Nowadays, the operating range of the turbines must be increased and more operation at off-design conditions is being requested. As a result, cavitation phenomena and their negative consequences are enhanced, which represents a potential threat for the hydropower plants. In fact, Francis turbines are the most common type of reaction machines in the power generation system. In addition, there are several cavitation patterns that can appear in the Francis turbine blades according to their location and morphology: (i) inlet leading edge cavitation; (ii) inter-blade vortex cavitation; and (iii) outlet traveling bubble cavitation [1].

To understand the fluid mechanic behavior of cavitation in the blades of a Francis turbine, numerical computations have been carried out using turbulence models coupled with homogeneous two-phase mixture models. The most popular mass transfer models are those developed by Kunz [2], Zwart [3] and Singhal [4]. The two latter models are both based on the simplified Rayleigh-Plesset equation of spherical bubble dynamics in an incompressible liquid, meanwhile the Kunz model is derived from Ginzburg-Landau theory. Among the various studies found on the numerical prediction of cavitation in Francis turbines, inter-blade vortex cavitation has been successfully captured with the unsteady RANS simulation with the SST-SAS turbulence model and the Zwart cavitation model [5].

There have been many attempts to investigate the flow structure and behavior of inlet blade cavitation in Francis turbines. For example, Avellan *et al.* [6] visualized the cavitation developments inside the medium-high specific speed GAMM Francis turbine runner for different Thoma's numbers. Based on these experimental results, Susan-Resiga *et al.* [7] and Escaler *et al.* [8] have carried out steady state numerical simulations that have predicted with good accuracy the cavitation shape and position in comparison with the experimental results.

In the present study, the unsteady simulation of the GAMM Francis turbine has been carried using the URANS turbulence model SST together with the Zwart cavitation model. Besides the best efficiency point (BEP), two other off-design operating conditions have also been taken into consideration to evaluate the leading edge cavitation unsteady behavior. Then, particular attention has been given to investigate the effect of flow perturbations at the

inlet and outlet of the runner only for the BEP.

EXPERIMENTAL DATA AND NUMERICAL SETUP

The runner geometry used in the present work corresponds to a Francis turbine model tested by the Laboratory of Hydraulic Machinery from the École Polytechnique Fédérale de Lausanne (EPFL), which was the test case of the GAMM Workshop on 3D Computation of Incompressible Internal Flows carried out in 1989. The model consisted of 24 stay vanes, 24 guide vanes and 13 blades, however, only the fluid domain around the runner without the distributor has been considered in our investigation. The domain inlet radius and width are 289 mm and 120 mm, respectively. To achieve a better numerical convergence, the draft tube outlet cone has been extended a length of 400 mm. The hill chart of GAMM Francis turbine has been obtained from the experiment data [6]. To simulate the characteristics of the leading edge cavitation in the turbine, three operation points corresponding to best efficiency point (BEP), part load and full load have been chosen. The corresponding performance parameters are listed in Table 1, where Q is the turbine volumetric flow rate, $\Omega = 52.36$ rad/s is the runner rotation speed, $R_{\text{ref}} = 0.2$ m is the reference radius of the runner, E is the specific hydraulic energy, T is the runner torque and η is the efficiency.

Table 1. Operating conditions simulated for the GAMM turbine.

Operating condition	Volume flow rate coefficient $\varphi = Q/\Omega\pi R_{\text{ref}}^3$ [dimensionless]	Energy coefficient $\psi = 2E/\Omega^2 R_{\text{ref}}^2$ [dimensionless]	Efficiency $\eta = T\Omega/\rho QE$ [dimensionless]
1	0.286	1.07	0.920
2	0.222	1.07	0.885
3	0.333	1.07	0.905

The SST turbulence model together with the Zwart-Gerber-Belamri cavitation model have been selected to simulate the unsteady flow field around the blades. The SST turbulence model has been treated near the wall using the automatic wall function proposed by Menter [9], which is the smooth blend of the linear and logarithm wall function. The treatment of the dissipation frequency, ω , has been addressed with the following Equations 1 to 4:

$$\omega_{\text{vis}} = \frac{6\nu}{0.075y^2}; \quad \omega_{\text{log}} = \frac{1}{0.3\kappa} \frac{u_\tau}{y} \quad (1)$$

$$\omega_I(y^+) = \sqrt{\omega_{\text{vis}}^2(y^+) + \omega_{\text{log}}^2(y^+)} \quad (2)$$

$$u_\tau^{\text{vis}} = \frac{U_1}{y^+}; \quad u_\tau^{\text{log}} = \frac{U_1}{\frac{1}{\kappa} \ln(y^+) + C} \quad (3)$$

$$u_\tau = \sqrt[4]{(u_\tau^{\text{vis}})^4 + (u_\tau^{\text{log}})^4} \quad (4)$$

where y is the wall normal distance of the first mesh grid and U_1 is the grid velocity. u_τ is the friction velocity and κ and C are the wall function constants. The *vis* and *log* superscripts mean viscous sublayer and logarithm layer, respectively.

Besides the SST turbulence model and its near wall treatment, the Zwart-Gerber-Belamri cavitation mass transfer model has been used to compute \dot{m} , as indicated in Equation 5:

$$\dot{m} = \begin{cases} -F_V \frac{3r_{\text{nuc}}(1-\alpha)\rho_v}{R_B} \sqrt{\frac{2}{3} \frac{P_V - P}{\rho_L}} & \text{if } P < P_V \\ F_C \frac{3\alpha\rho_v}{R_B} \sqrt{\frac{2}{3} \frac{P - P_V}{\rho_L}} & \text{if } P > P_V \end{cases} \quad (5)$$

where F_V and F_C are the empirical coefficients of vaporization and condensation, respectively, r_{nuc} is the nucleation volume fraction and R_B is the typical bubble radius. In this work, the empirical parameters have been set to their default values, i.e., $F_V = 50$, $F_C = 0.01$, $r_{\text{nuc}} = 5 \cdot 10^{-4}$ and $R_B = 2 \cdot 10^{-6}$ m. The rest of the variables in Equation

5 are the vapor volume fraction, α , and the local pressure, P . The rest of constants in Equation 5 are the vapor density, $\rho_v = 0.02308 \text{ kg/m}^3$, the water liquid density, $\rho_L = 997 \text{ kg/m}^3$, and the water saturation pressure, $P_V = 3169 \text{ Pa}$.

The inlet fluid domain has been defined as a Dirichlet boundary condition with specific velocity components in a cylindrical coordinate system corresponding U_u (tangential), U_r (radial) and U_z (axial). In particular, the inlet U_z has been set to zero and the U_r and U_z have been derived from the inlet velocity triangle with the assumption that the flow angle is equal to the guide vane angle. Based on this, the velocity components under different operating points have been calculated and they are listed in Table 2.

The fluid domain outlet boundary has been set as an opening and the entrainment pressure, P_{out} , has been fixed with a value calculated using the Thoma's cavitation number [10] expressed with Equation 6:

$$\sigma = \frac{P_{out} - P_V}{\rho_L g E} \quad (6)$$

where E is the output power of the turbine, which can be deduced from the turbine efficiency plotted in the hill chart. In order to compare the cavitation unsteady flow behavior under different operation conditions, we have kept σ constant and equal to 0.14.

Table 2. Fluid domain inlet and outlet boundary conditions under different operation conditions.

Operating condition	Inlet boundary			Outlet boundary
	U_z [m/s]	U_r [m/s]	U_u [m/s]	P_{out} [Pa]
1	0	1.94	4.39	11326
2	0	1.53	4.86	11326
3	0	2.30	3.83	11326

MODEL VALIDATION

Menter *et al.* [9] investigated the influence of using different y^+ values with the SST turbulence model because it uses the blending wall function, and they found that the SST model is not very sensitive to the mesh size. However, recent studies focused on two-phase flows carried out by Decaix [11] and Picardi *et al.* [12] have found that the mesh grid resolution may have a significant influence on the simulation results. Therefore, we have conducted some tests to evaluate the effects of the grid refinement and element density in our results.

The steady state no cavitation results simulated with different meshes in terms of number of elements and y^+ values have been compared for the BEP condition. All the meshes have been generated using the ANSYS® Turbogrid tool with a similar increase ratio around 2.8. Because only a single runner channel has been considered in the fluid domain, the coarsest mesh only consisted of around 127,000 hexahedrons with higher refinement in both the blade and the shroud walls, as shown in Figure 1a. Among the six meshes shown in Figure 1, those corresponding to (a), (b) and (c) have y^+ values above 11.35 and, therefore, the first grid point is located within the logarithm boundary layer. Meanwhile, for meshes corresponding to (d), (e) and (f), the y^+ values are below 1 and, therefore, the first grid point is located within the viscous sublayer.

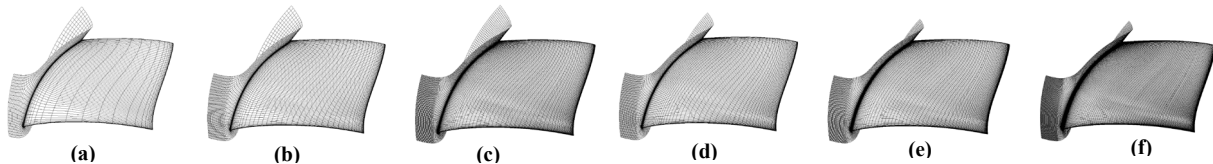


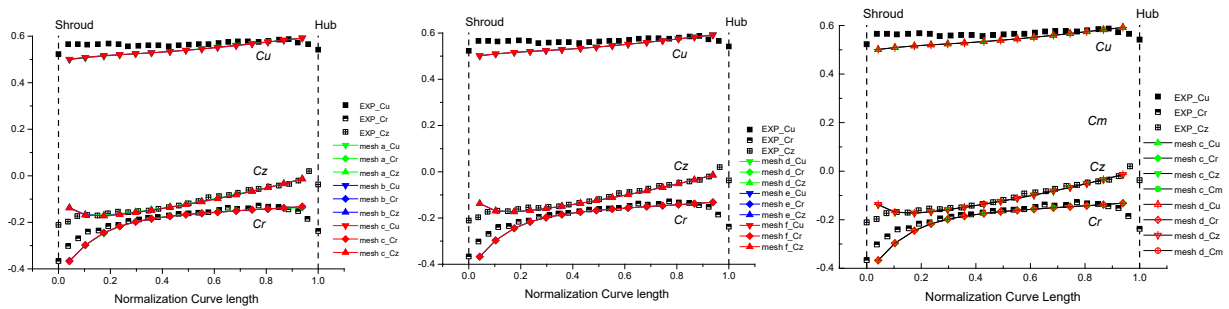
Figure1: Tested meshes with different levels of refinement.

The torque values calculated with the various meshes at BEP are summarized in the Table 3. All of them present a good level of accuracy compared to the experimental value of 388 N m. A local analysis of the mesh influence has been carried out comparing the numerical velocity profiles at the runner inlet with the measured ones as shown in

Figure 2, where the tangential, radial and axial velocity coefficient are calculated as $C_u = \frac{U_u}{\sqrt{2E}}$, $C_r = \frac{U_r}{\sqrt{2E}}$ and $C_z = \frac{U_z}{\sqrt{2E}}$, respectively. The overall good agreement between them is confirmed. In more detail, very good predictions are found in the main streamflow.

Table 3. Summary of the simulation results obtained with the different meshes plotted in Figure 1.

Name	Mesh number	Average y^+ around Runner	Average y^+ around Shroud	Runner torque [Nm]
a	127000	36.01	52.92	387.6
b	382000	17.3	22.6	387.1
c	1187000	42.8	32.25	386.6
d	1192000	0.54	0.78	389.8
e	3184000	0.53	1.27	390.8
f	8753000	0.26	0.75	391.7



(a) different grid resolution with high y^+ (b) different grid resolution with low y^+ (c) same grid resolution with different y^+

Figure 2: Comparison between the experimental velocity profiles and the predicted ones for different grid resolutions and y^+ values.

Two of the meshes with different y^+ , corresponding to c and d in Figure 1, have been selected to simulate the leading edge cavitation for decreasing cavitation numbers. The corresponding torque values are shown in Figure 3. They present a good similarity between the two meshes, which indicates that the numerical simulation of the cavitation is not significantly influenced by the y^+ value.

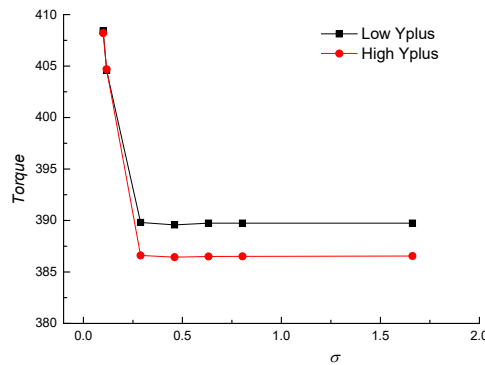


Figure3: Calculated torque as a function of σ with two meshes having different y^+ values.

RESULTS WITH UNIFORM AND STEADY FLOW CONDITIONS

To carry out the unsteady RANS simulation of the cavitation, the Reboud’s density correction for the eddy viscosity [13] has been implemented on the ANSYS® CFX platform. Besides, the numerical settings for the unsteady calculation have been the following ones:

- a time step of 10^{-4} s, that results in a maximum Courant-Friedrichs-Lewy (CFL) value equal to 5 at BEP,
- 50 loop iterations and a convergence level of 10^{-6} .

The unsteady calculation results have been summarized in Table 4 for different discharges. In all the cases, the pressure near the aft region of the cavity is kept almost constant, as well as the cavity length and shape. No obvious cavitation instabilities occur in any of the operating points. These results seem indicate that, without considering internal flow perturbations inside the fluid domain or at the boundaries, the inlet leading edge cavitation is a rather stable cavitation structure inside a Francis runner operating at BEP or at lower or higher flow rate.

Table 4. Summary of the unsteady cavitation simulations under different operation conditions.

Operation point	Inlet blade angle [degree]	Relative velocity [m/s]	Cavitation length [m]	Cavitation thickness [m]	Shedding frequency [Hz]
1	12.6	8.90	0.141	0.0117	Not detected
2	18.8	9.30	0.069	0.0048	Not detected
3	14.5	9.36	0.158	0.0124	Not detected

RESULTS WITH FLOW PERTURBATIONS

Although the leading edge cavitation in Francis turbine appears to have stable behavior under uniform and steady flow conditions inside the runner, the actual flow will present various types of flow perturbations, which might force a significant cavity oscillation or shedding process. The two main flow perturbation inside the runner are caused by: (i) the rotor stator interaction at the gap between the guide vanes and the runner blades; and (ii) the draft tube vortex rope [14].

A mathematical expression, as indicated in Equation 7, has been used to model the perturbation at the runner inlet velocity distribution induced by the guide vanes' wakes as outlined in Figure 4:

$$\vec{V}(\theta, t) = \vec{C}(1 + A\cos(2\pi f_s t + 2\pi\theta/\theta_s)) \quad (7)$$

where $\vec{V}(\theta, t)$ is the absolute velocity distribution at the runner inlet, $\vec{C} = (1.94, 4.39, 0)$ is the uniform absolute velocity in cylindrical coordinates at the runner inlet at BEP, A is the perturbation level of the velocity distribution, which is specified equal to 0.5, f_r is the guide vane passing frequency, $2\pi\theta/\theta_s$ is the inter blade phase difference, and θ_s is the angle between two guide vanes. This velocity distribution is a simplification of the real one observed in the runner and it neglects the runner cascade influence and the dynamic effects [14].

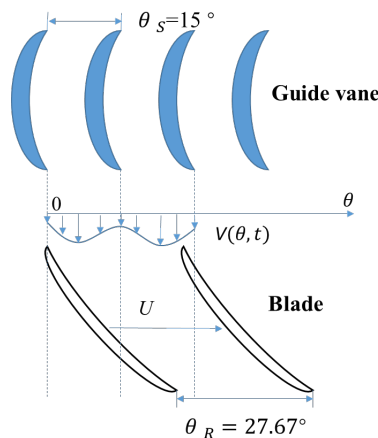


Figure 4: Velocity distribution at the runner inlet induced by the RSI.

In presence of the draft tube, there is a vortex rope that develops at loads above or below the BEP. The vortex rope is induced by the residual tangential velocity component in the draft tube. At part load, the vortex rope may provoke a low frequency pressure fluctuation at the outlet of the runner. This frequency is called the Rheingans [15] frequency, f_R , that is proportional to the rotation frequency, f_N , and that typically ranges from $f_N/3.6$ to $f_N/3$.

Therefore, in our case the pressure fluctuation is considered to develop at a frequency of 2.5Hz and its amplitude is considered to be the 10% of P_{out} . Therefore, to predict the behavior of the leading edge cavitation when the vortex rope exists, an oscillatory pressure signal has been set at the outlet boundary of the fluid domain as defined with the following expression $P_{out} = 11326 (1 + 0.1 \cdot \sin(2\pi f_N t))$.

The work of Tsujimoto *et al.* [16] predicts that two types of cavitation instabilities can occur in Francis turbines corresponding to the following models:

- model 1: the height of the attached cavitation sheet becomes unstable due to a high frequency perturbation,
- model 2: the length of the attached cavitation sheet becomes unstable due to a low frequency perturbation.

A sketch of the two different types of cavitation instability is shown in Figure 5.

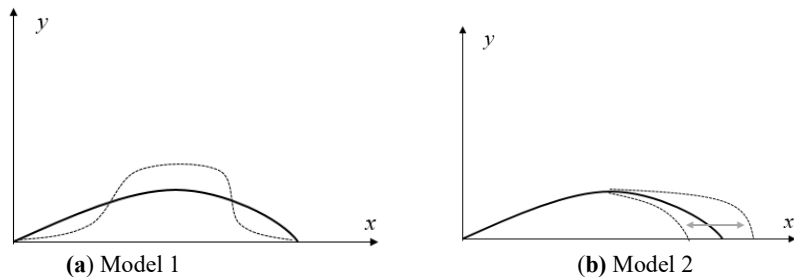


Figure 5: Instabilities of the attached cavitation sheet induced by external perturbations of high (a) and low (b) frequency as predicted by Tsujimoto *et al.* [16].

The evolution in time of the leading edge cavitation vapor volume fraction on the suction side of the runner blade at a span of 0.95 is presented in Figure 6. When the wake of the guide vanes disturbs the inlet flow to the runner blades and generates a high frequency perturbation, the cavity length remains constant meanwhile the chord wise cavity height fluctuates. This behavior shown in Figure 6a would correspond to the model 2 instability. When the pressure frequency fluctuates at the outlet boundary due to the vortex rope, the cavity length fluctuates meanwhile the chord wise cavity height remains constant. This behavior shown in Figure 6b would correspond to the model 1 instability.

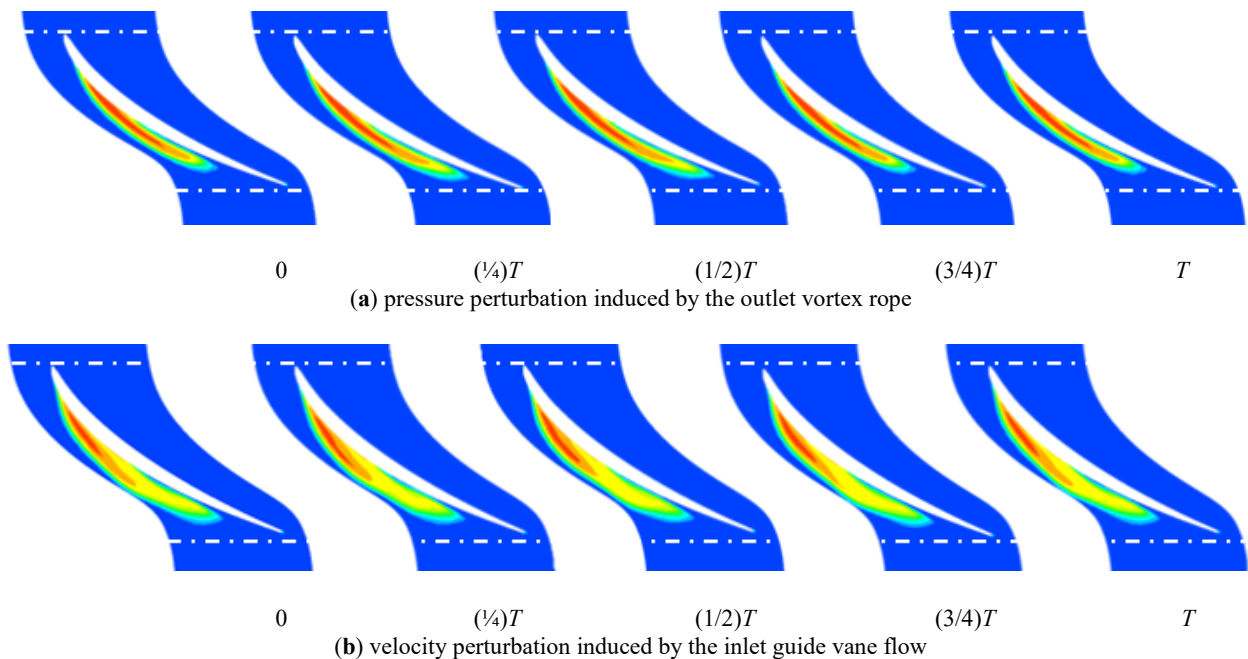


Figure 6: Contours of vapor volume fraction at different instants of the instability period, T , induced by a perturbation of the outlet pressure (a) and of the inlet velocity distribution (b).

These two cavitation instabilities can be described with a simple 1D model [17] that assumes a vapor cavity in a duct of a given section A and inlet length L and of infinite outlet length. From the mass and momentum conservation equations, the relationship between the pressure, p , and the cavity volume, V_c , is given by Equation 7:

$$\frac{A}{\rho_L L} p = \ddot{V}_c \quad (7)$$

Given a pressure fluctuation with frequency f defined by $p = e^{i2\pi f t}$, then Equation 7 can be solved and Equation 8 is obtained:

$$V_c = V_{c0} - \frac{1}{(\lambda 2\pi f)^2} e^{i2\pi f t} \cdot \left(\frac{A}{\rho_L L}\right) \quad (8)$$

where the V_{c0} is initial cavity volume, and the second term in the expression is the fluctuation of the cavity volume.

According to Equation 8, the amplitude of the cavity volume fluctuation is proportional to $1/f^2$. Therefore, for large values of λ such as in the case of the high frequency inlet pressure fluctuation, induced by the inlet velocity distribution, the cavity volume fluctuation will be small. This result can be confirmed in Figure 7 where the dimensionless cavity length has been plotted as a function of the fluctuation period, T , for the 200 Hz inlet perturbation. It can be seen that the cavity length is constant and the unstable behavior only affects the lateral surface of the cavity, which corresponds to model 1. However, for the 2.5 Hz pressure perturbation corresponding to a low values of λ , the cavity volume fluctuation amplitude is significant and leads to an obvious perturbation of the cavity length, which corresponds to model 2.

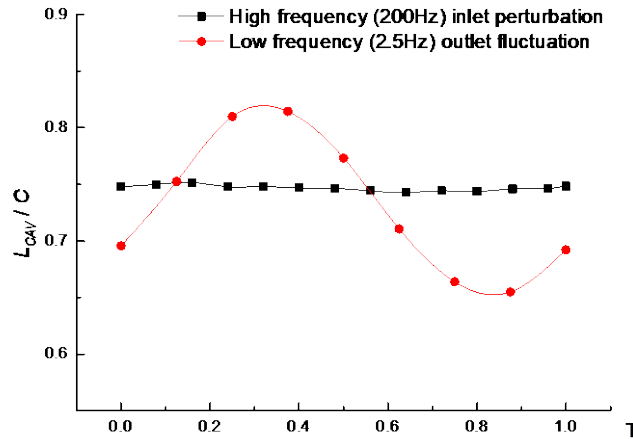


Figure 7: The dimensionless cavitation length fluctuation for high frequency inlet and low frequency outlet perturbations.

CONCLUSION

First, steady simulations of the leading edge suction side cavitation in the GAMM Francis turbine blades have been carried out with the SST turbulence model and the Zwart cavitation mass transfer model using various meshes. It has been confirmed that the results are not sensitive to the mesh resolution for the cases considered in our study.

Then, unsteady simulations with uniform boundary conditions in terms of inlet velocity and outlet pressure have demonstrated that the attached partial cavity behaves as a stable structure without any significant fluctuation at three different operating conditions including BEP, part load and high load.

Finally, the effects of flow perturbations on the cavitation dynamic behavior have been evaluated at BEP. On one hand, it has been found that a high frequency inlet velocity fluctuation, as that induced by the guide vanes outlet flow, provokes an instability of the cavity surface. On the other hand, a low frequency outlet pressure fluctuation, as that induced by the rotating vortex rope, provokes an instability of the cavity length.

As a future work, the fluid domain comprising the runner will be enlarged to take into account the stay vanes, the guide vanes and the draft tube cone using the transient blade row modelling approach in order to verify the present

conclusions.

ACKNOWLEDGEMENTS

The present research work was financially supported by China Scholarship Council.

REFERENCES

- [1] Avellan F. Introduction to cavitation in hydraulic machinery[C], The 6th International Conference on Hydraulic Machinery and Hydrodynamics, Timisoara, Romania. 2004.
- [2] Kunz R F, Boger D A, Stinebring D R. A preconditioned Navier–Stokes method for two-phase flows with application to cavitation prediction[J]. *Computers & Fluids*, 2000, 29(8): 849-875.
- [3] Zwart P J, Gerber A G, Belamri T. A two-phase flow model for predicting cavitation dynamics[C], Fifth international conference on multiphase flow, Yokohama, Japan. 2004.
- [4] Singhal A K, Athavale M M, Li H, Jiang Y. Mathematical basis and validation of the full cavitation model[J]. *Journal of fluids engineering*, 2002, 124(3): 617-624.
- [5] Yamamoto K, Müller A, Favrel A, Avellan, F. Experimental evidence of inter-blade cavitation vortex development in Francis turbines at deep part load condition[J]. *Experiments in Fluids*, 2017, 58(10): 142-154.
- [6] Avellan F, Dupont P, Farhat M, Gindroz B, Henry P, Hussain M, Santal O. Experimental flow study of the GAMM turbine model[M], 3D-Computation of Incompressible Internal Flows. Vieweg+ Teubner Verlag, 1993: 33-53.
- [7] Susan-Resiga R, Muntean S, Anton I, Bernard S. Numerical investigation of 3D cavitating flow in Francis turbines[C], Conference on Modeling Fluid Flow (CMFF'03), The 12th International Conference on Fluid Flow Technologies, Budapest, Hungary. 2003.
- [8] Escaler F X, Roig R, Hidalgo V. Sensitivity analysis of Zwart-Gerber-Belamri model parameters on the numerical simulation of francis runner cavitation[C], CAV2018: Baltimore, USA, 14-16 May 2018.
- [9] Menter F, Carregal Ferreira J, Esch T, Konno B. The SST Turbulence Model with Improved Wall Treatment for Heat Transfer Predictions in Gas Turbines [C], Proceedings of the International Gas Turbine Congress, Tokyo, Japan, 2003.
- [10] Nilsson H, Davidson L. Validations of CFD against detailed velocity and pressure measurements in water turbine runner flow[J]. *International Journal for Numerical Methods in Fluids*, 2003, 41(8): 863-879.
- [11] Goncalves E and Decaix J. Wall model and mesh influence study for partial cavities[J]. *European Journal of Mechanics-B/Fluids*, 2012, 31: 12-29.
- [12] Picardi R, Zhao L, Battaglia F. On the ideal grid resolution for two-dimensional eulerian modeling of gas–liquid flows[J]. *Journal of Fluids Engineering*, 2016, 138(11): 114503.
- [13] Coutier-Delgosha O, Fortes-Patella R, Reboud J L. Evaluation of the turbulence model influence on the numerical simulations of unsteady cavitation[J]. *Journal of Fluids Engineering*, 2003, 125(1): 38-45.
- [14] Pål Henrik Enger Finstad. Secondary flow fields in Francis turbines: mapping and analyzing dynamics in rotor-stator interaction and draft tube flow with novel methods [D] .Ph.D Thesis, Trondheim, Norwegian University of Science and Technology, 2012.
- [15] Rheingans W J, Milwaukee, W. Power swings in hydroelectric power plant [J]. *Transactions of the ASME*, 1940, 63(3):171-184.
- [16] Horiguchi H, Watanabe S, Tsujimoto Y. A linear stability analysis of cavitation in a finite blade count impeller[J]. *Journal of fluids engineering*, 2000, 122(4): 798-805.
- [17] Duttweiler M E, Brennen C E. Surge instability on a cavitating propeller[J]. *Journal of Fluid Mechanics*, 2002, 458: 133-152.